The Effect of Nitrogen Ion Implantation on the Photoactivity of TiO_2 Rutile Single Crystals

Oliver Diwald,[†] Tracy L. Thompson,[†] Ed G. Goralski,[‡] Scott D. Walck,[‡] and John T. Yates, Jr.*[,†]

Surface Science Center, Department of Chemistry, University of Pittsburgh, Pittsburgh, Pennsylvania 15260, and Pittsburgh Plate Glass Industries, Inc., Glass Technology Center, Pittsburgh, Pennsylvania 15238

Received: April 28, 2003; In Final Form: July 17, 2003

The effect of impurity doping on the photoactivity of TiO_2 rutile single crystals was subjected to a combined surface-science and bulk-analysis study. The incorporation of nitrogen ions, N^-, into TiO_2 single crystals was achieved by sputtering with N_2^+/Ar^+ mixtures and subsequent annealing to 900 K under ultrahigh vacuum conditions. This procedure leads to a 90 Å thick structurally modified near-surface region, which, by the use of cross sectional transmission electron microscopy, can be described as rutile grains imbedded within a monocrystalline strained rutile matrix. The presence of N^- ions distributed in the first 200 Å below the surface was revealed by X-ray photoelectron spectroscopy, in agreement with sputter depth profiles obtained by secondary ion mass spectroscopy. The concentration of N^- doping is about 10^{20} cm^{-3} in the first 200 Å of the near-surface region. The photodesorption of O_2 was employed to study the changes in the photochemical properties of nitrogen-implanted crystals. The action curves for O_2 photodesorption exhibit an unexpected blueshift compared to undoped crystals. The effect is attributed to the deposition of electronic charge in the lower levels of the conduction band (band-filling mechanism), causing allowed indirect photoexcitation processes to shift to energies higher than the band gap.

I. Introduction

Titanium dioxide (TiO_2) is a promising material for many photochemical applications spanning the range from photoelectrochemical splitting of water into hydrogen and oxygen[1,2] and wet solar cells[3] to photocatalysis.[4−6] TiO_2 has long-term stability, is a nontoxic material, and is relatively inexpensive. A major goal in the development of TiO_2-based materials is to extend the photoactivity from 3.0 eV into the range of visible light in order to utilize solar light more efficiently. It is widely recognized that the electrical and photophysical properties of oxide materials are strongly influenced by electronic states associated with defects and dopants. Model studies of single-crystal oxides have yielded a rich body of information about electronic states associated with oxygen anion vacancies. This is especially true for rutile TiO_2(110), which serves as a prototype of a single-crystal transition-metal-oxide surface.[7]

Most work on the electronic defects associated with impurity dopants has been restricted to polycrystalline materials. Recently, different groups have reported that substitional doping with nonmetal atoms such as carbon,[8] sulfur,[9] and nitrogen[10−12] in the TiO_2 lattice shifts the absorption edge to lower energies. For example, Asahi et al. reported that films and powders of $TiO_{2-x}N_x$ reveal a dramatic improvement over pure titanium oxide under visible light in their optical absorption and the level of photocatalytic activity.[11,12] The authors claim that nitrogen doped into substitutional sites of TiO_2 has proven to be indispensable for "band gap narrowing".

The aim of this study was to investigate the influence of substitutional nitrogen doping on the photoactivity of the rutile TiO_2(110) single-crystal surface. The structure and chemical composition of the nitrogen-doped near-surface region were investigated with cross-sectional transmission electron microscopy (XTEM), secondary ion mass spectrometry (SIMS), and X-ray photoelectron spectroscopy (XPS) in conjunction with sputter depth profiling. The doping effect on the photoactivity was measured by the photodesorption of oxygen performed under controlled ultrahigh vacuum (UHV) conditions. It will be shown that incorporation of N^- ions with a concentration of about 1 atomic % into the rutile lattice can be achieved by sputtering with a mixture of N_2^+ and Ar^+ ions. After subsequent annealing to 900 K, the TiO_2 becomes electronically reduced and adsorbs oxygen on its surface. The photodesorption of oxygen, measured as a function of UV excitation energy, revealed an unexpected blueshift effect compared to undoped rutile single crystals.

II. Experimental Section

Sample preparation of the nitrogen-doped TiO_2(110) single crystals, Auger electron spectroscopic analysis, as well as the temperature-programmed desorption and photodesorption studies were carried out in a stainless steel UHV chamber with a base pressure of $<2 \times 10^{-10}$ Torr. Details of the experimental apparatus and the method for performing the O_2 photodesorption experiments are described elsewhere.[13]

Crystals used for this investigation were obtained from Princeton Scientific Corportation with dimensions of 10 mm $\times$ 10 mm $\times$ 1 mm and with precut slots around all four edges in order to directly mount the crystal on a Ta support plate using Ta foil clips. A type-K thermocouple is embedded inside the corner of the TiO_2 crystal by using a ceramic adhesive (Aremco 571) to hold it inside of a diagonal slot. The mounting of the crystal is done in such a way that only the front face of the crystal is exposed to the 1.6 mm diameter aperture leading to

* Author to whom correspondence may be addressed. E-mail: jyates@pitt.edu.
[†] University of Pittsburgh.
[‡] Pittsburgh Plate Glass Industries, Inc.

10.1021/jp030529t CCC: $27.50
Published on Web 12/11/2003

the differentially pumped quadrupole mass spectrometer (QMS) during measurements or during dosing with the calibrated molecular beam doser. Resistive heating is done by passing current through two tungsten wires (0.38 mm diameter) that are directly spot welded to the back of the Ta support plate. Mounting in this manner allows for sample cooling to temperatures of 110 K and heating to 1100 K. Prior to sputter treatment with 3 keV ions (Ar^+ ions or mixtures of Ar^+ and N_2^+ ions), the crystals are cleaned by successive intervals of Ar^+ sputtering (1.5 kV) followed by full oxidation in O_2 at 900 K followed by cooling in O_2. This has been done until no traces of impurities were measured using Auger electron spectroscopy.

XPS and SIMS measurements were carried out at the Pittsburgh Plate Glass Technology Center. XPS spectra were acquired with an ESCALAB Mk II (Vacuum Generators) spectrometer using unmonochromatized Mg Kα X-rays (240 W). Cycles of XPS measurements and subsquent Ar^+ sputtering steps (4 keV, $I = 4\ \mu A/cm^2$) were done in a high-vacuum chamber with a base pressure of 10^{-8} Torr until a profile for nitrogen content vs sputter time was obtained. The binding energy of the N (1s) peaks was calibrated with respect to the O (1s) peak at 530.2 eV. The nitrogen concentration was estimated from the relative area intensities of the N (1s), Ti (2p), and O (1s) peaks. They were normalized with respective relative sensitivity factors in the Vacuum Generators software package. Dynamic SIMS experiments were performed in positive mode with 5 keV Ar^+ ions and a measured ion current density of $I = 1.25\ \mu A/cm^2$.

XTEM samples were prepared using the small-angle cleavage technique.[14] All samples were cleaned in a radio frequency coupled Ar/O_2 plasma. The transmission electron microscope was a 200-kV field-emission gun instrument (Philipps Tecnai F20) located at the Material Research Center at Carnegie Mellon University. Photodesorption studies were carried out using a 500-W high-pressure mercury lamp and a series of spectral filters with 10 nm wide pass energies. The radiation intensity was measured using a thermopile detector (Oriel 71751) as a primary standard over the spectral region of interest.

III. Results

A. Implantation of Nitrogen and Determination of its Concentration and Depth Distribution. Implantation of nitrogen into the lattice of TiO_2 crystals was done by sputtering with a gas mixture of 80% nitrogen and 20% Ar at room temperature and an acceleration voltage of 3 kV.[15] The total fluence of ions incident to the crystals during the sputtering process was 10^{17} ions/cm^2. For comparison, a reference crystal was treated in the same way with Ar^+ ions alone and subsequently subjected to the same treatment and experiments as the nitrogen-implanted sample. All crystals were annealed at 900 K for 3−5 h in UHV after sputtering. For the nitrogen-implanted sample, Auger electron spectroscopy was used to provide evidence for incorporated nitrogen. Since only the nitrogen KLL transition is seen, and its energy overlaps the titanium LMM transition located at 380 eV, the relative ratio for the Ti LMV (420 eV)/Ti LMM transitions was used to obtain an estimate of N concentration. A broad optical absorption from 1500 nm to almost 400 nm associated with electronically reduced defects in the bulk (e.g., color centers) was measured on the nitrogen-implanted sample and is similar to that observed for undoped crystals. These are typical effects for TiO_2 single crystals and originate from extensive annealing under UHV conditions.[7] Additional sharper absorption bands that may originate from beneficial nitrogen doping were not observed above $\lambda = 400$ nm ($h\nu < 3$ eV).

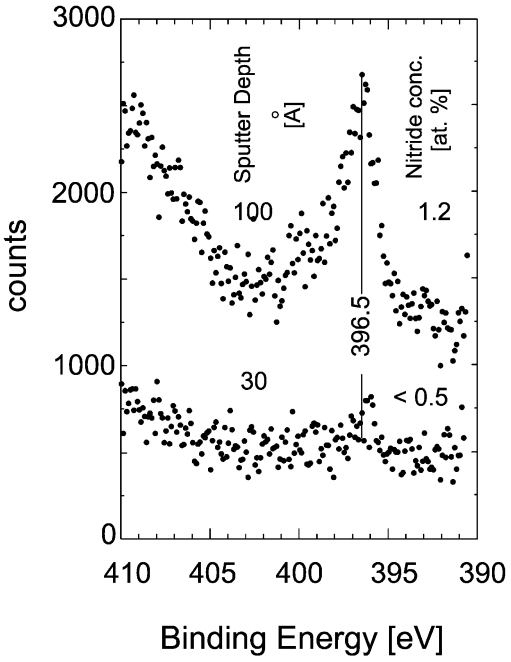

Figure 1. Nitrogen (1s) spectrum from a nitrogen-implanted TiO_2-(110) crystal at two different Ar^+ sputter depths.

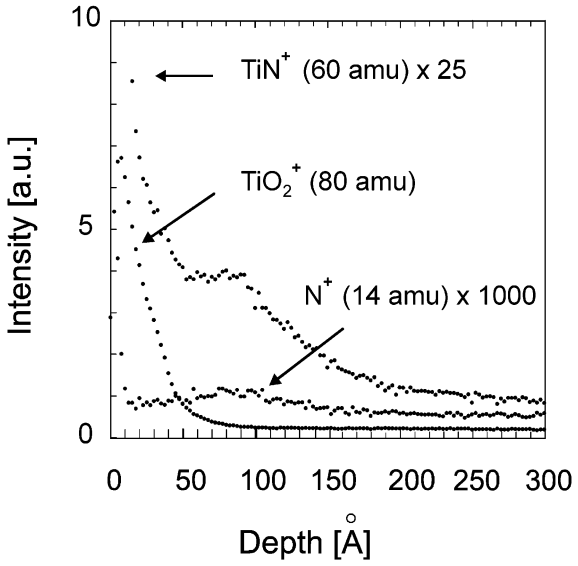

Figure 2. SIMS profile of nitrogen-implanted TiO_2(110) crystal.

For the quantification of the implanted nitrogen and the determination of its chemical nature, XPS was employed. No evidence of nitrogen was observed at the surface. However, by use of sputter depth profiling, an XPS feature centered at 396.5 eV can be observed after removal of the first 30 Å from the surface (Figure 1). It is assigned to the N (1s) transition of chemically bound N^- species within the crystalline TiO_2 lattice.[11,12,16]

The depth distribution of nitrogen species was determined by XPS using Ar^+ sputter depth profiling. The resulting profile (not shown) was in good agreement with the nitrogen profile obtained by SIMS (Figure 2). For comparison, the masses 80 (TiO_2^+), 14 (N^+), and 60 (TiN^+) were recorded.[17] The nitrogen signal (14 amu) and the titanium nitride signal (60 amu) exhibit a maximum at approximately 90 Å beneath the surface. At this depth, the nitrogen concentration was 1.2 ± 0.5 atomic % as determined by XPS. The two surface analysis methods agree

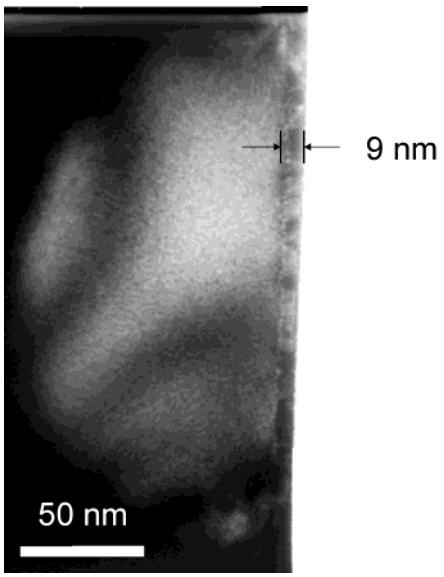

Figure 3. Low magnification TEM image of the cross section of the nitrogen-implanted single crystal.

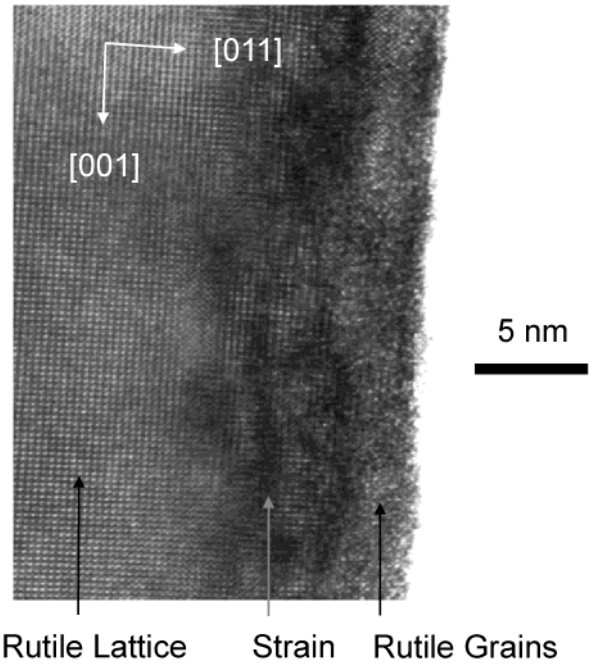

Figure 4. Cross-sectional high-resolution TEM image of the nitrogen-implanted crystal. On top of the monocrystalline rutile lattice are recrystallized rutile grains. The blackened regions in the image indicate lattice strain.

with the implanted N^- species being present with a maximum concentration at a depth of about 90 Å.

B. Transmission Electron Microscopy Cross Sections. The structure of the near-surface region of ion-sputtered and post-annealed (at 900 K) TiO_2 crystals was investigated by XTEM. A low-magnification image of the nitrogen-implanted sample is shown in Figure 3. In contrast to similar images obtained from the undoped crystal (not shown), an outer layer with varied contrast compared to the bulk underneath is clearly observable. Its thickness was uniform and about 90 Å in size. (X-ray reflectivity measurements, performed on the same sample, indicated the presence of a 88 ± 4 Å thick upper layer of elastically strained rutile.)[18] A high-resolution TEM image in Figure 4 provides an example of the structural changes of this outer layer. The image reveals the transition from the mono-

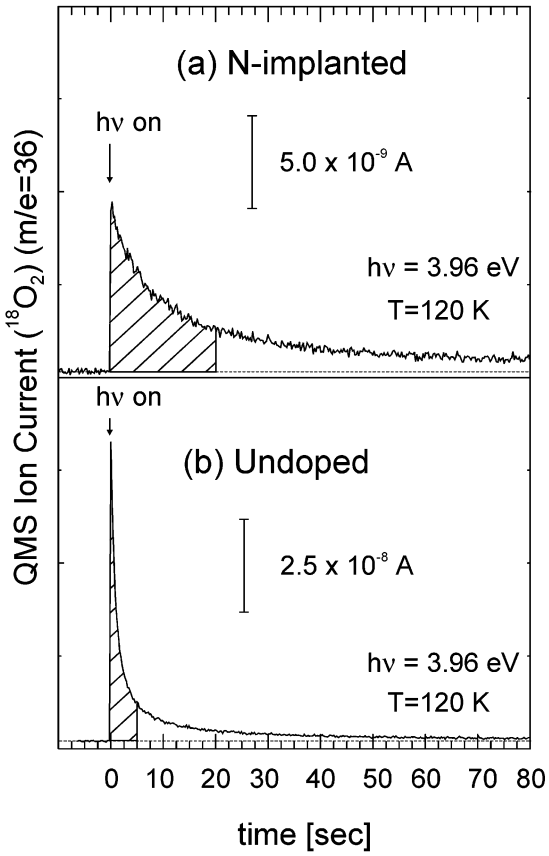

Figure 5. Time-dependent $^{18}O_2$ desorption signal for (a) a nitrogen-implanted and (b) an undoped TiO_2(110) crystal. Total oxygen exposure was 1×10^{15} molecules cm^{-2} causing saturation coverage. The photon flux at 3.96 eV, $F_{h\nu}$, was 1×10^{15} photons cm^{-2} s^{-1}. The crosshatched areas show the integration range employed in measuring the photodesorption yield.

crystalline bulk crystal structure through an area of strain (darker average contrast) to a polycrystalline grain structure in the near-surface region.

The presence of many structural defects prevented imaging of the atomic structure of the grains in detail in the near-surface region. However, the contrast differed substantially from that expected for an amorphous region and local fringes from atomic columns were visible. Fourier transforms were used to determine *d* spacings and orientations in the polycrystalline surface region and were calibrated relative to the bulk rutile regions. Only patterns that were consistent with rutile were seen. The rutile grains that were analyzed in the near-surface region were 20−70 Å in size.

C. O_2 Photodesorption and the Photoaction Curve. The TiO_2 crystals were heated to 900 K to reproducibly generate a surface oxygen anion vacancy concentration between 5 and 10% of a monolayer.[7,19,20] Under UHV conditions, the chemisorption of oxygen can only occur on TiO_2 surfaces with anion vacancies (accompanied by electronically reduced cationic sites).[13,20] O_2 adsorption at 120 K leads to the formation of chemisorbed oxygen which, on the basis of high-resolution electron energy loss spectroscopy, was assigned to O_2^- species.[21] When these samples are exposed to UV radiation, O_2 photodesorption takes place. This process is explained by the photogeneration of holes and concomitant electronic neutralization of the O_2^- species causing O_2 desorption. Molecular oxygen, released from the surface, is then detectable by the line-of-sight QMS.

Figure 5 contains typical O_2 photodesorption signals measured on vacuum annealed samples, which were previously sputtered

with a mixture of N_2^+ and Ar^+ ions (nitrogen-implanted, Figure 5a) and samples sputtered only with Ar^+ ions (undoped, Figure 5b). For the nitrogen-implanted material, a much longer decay time was observed. (The signal in Figure 5a is multiplied by a factor of 5.) The time constants for both curves were obtained by curve fitting to eq 1

$$N_{O_2} = N_{O_2}{}^0 \exp(-F_{h\nu} Q t) \quad (1)$$

where N_{O_2} is the O_2 coverage during photodesorption, $N_{O_2}{}^0$ is the initial coverage of O_2, $F_{h\nu}$ is the photon flux at 3.96 eV, t is the UV irradiation time, and Q is the cross section for photodesorption of O_2. The photodesorption signal, measured on the nitrogen-implanted sample (Figure 5a), occurs with a cross section of 10^{-16} cm^2, 1 order of magnitude smaller than that for the process observed on undoped TiO_2(110) ($Q = 10^{-15}$ cm^2, Figure 5b). Both photodesorption processes were observed in previous studies on vacuum-annealed rutile TiO_2(110) crystals.[13] The relative ratio between these two processes and, thus, the shape of the photodesorption signal strongly depend on the morphology of the TiO_2(110) surface. For example, O_2 photodesorption from a crystal that was Ar^+ sputtered and annealed at 900 K for a limited period of time (i.e., $t = 1-2$ h) occurs preferentially via the slow-decaying process with a cross section of 10^{-16} cm^2. After longer annealing times ($t > 3$ h), the contribution of the fast-decaying process with a cross section of 10^{-15} cm^2 dominates the overall shape of the photodesorption signal, which does not change with further annealing. Thus, the difference in the signals of Figure 5 are explained by the disordered surface structure of the nitrogen-implanted crystal, also indicated by the XTEM image in Figure 4.

Action curves for the process of O_2 photodesorption were measured to determine the effect of nitrogen implantation on the spectral response of the TiO_2(110) single crystals. Before each experiment, the crystal was annealed to 900 K momentarily, and a constant exposure (1×10^{15} molecules cm^{-2}) of O_2 was dosed after the crystal cooled to 120 K. The relative yield ($Y_{h\nu}$) of photodesorbed oxygen as a function of the excitation energy, $h\nu$, was determined by ratioing the integral intensity of the photodesorption signal to the incident photon fluence according to eq 2

$$Y_{h\nu} = \frac{\int_0^{t_1} \Delta P_{O_2} \, dt}{\int_0^{t_1} F_{h\nu} \, dt} \quad (2)$$

For higher accuracy, the integration time for the slower-decaying processes on nitrogen-implanted TiO_2 was 20 s, whereas for the undoped samples, only the first five seconds were used (see crosshatched areas in Figure 5). Both action curves in Figure 6 were normalized to the photodesorption yield measured at an energy of 4.1 eV in order to show differences in their energy dependence. It can be clearly seen that for the crystal exclusively sputtered with Ar^+ ions (and annealed to 900 K), the threshold energy for O_2 photodesorption is at about 3.0 eV. This value corresponds to the effective band gap of bulk rutile and is in very good agreement with previous studies performed on TiO_2-(110) crystals, which were reoxidized in oxygen flux after sputter cleaning and then vacuum annealed to reproducibly produce surface defects.[7,13,20]

When exactly the same sputter and annealing process was carried out with a $N_2^+ + Ar^+$ mixed ion beam, the action curve for O_2 photodesorption was dramatically shifted to the blue, as seen in Figure 6. The threshold energy at about 3.2 eV is shifted

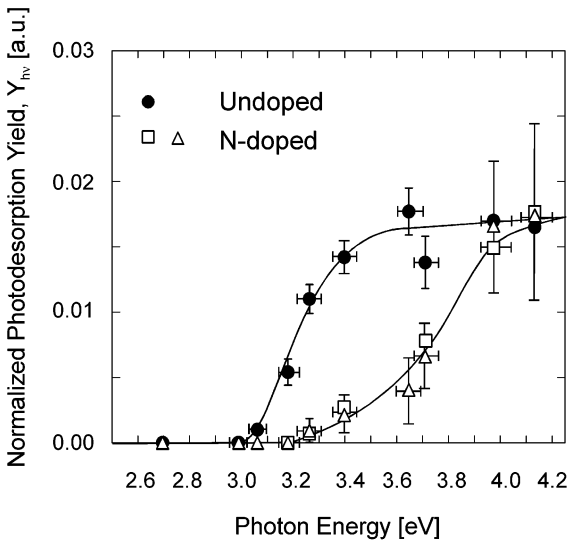

Figure 6. The photoaction curve for O_2 photodesorption from vacuum annealed TiO_2(110) surfaces. The integrated photodesorption magnitude at each energy has been divided by the photon flux at each respective energy to obtain $Y_{h\nu}$. Both types of photoaction curves were normalized to the photodesorption yield measured at 4.1 eV. Open squares and triangles represent values that were measured independently on two different nitrogen-doped single crystals.

in the *opposite* direction to that reported by Asahi et al.[11,12] for nitrogen-doped polycrystalline TiO_2. Thus two profound differences are observed for TiO_2(110) crystals containing N^- substitutional impurities compared to identical crystals prepared without N^- incorporation:

1. The O_2 photodesorption cross section for the nitrogen-implanted crystals decreases by a factor of 10, from 10^{-15} cm^2 to 10^{-16} cm^{-2}, for 3.96 eV photons.

2. The threshold for O_2 photodesorption increases by 0.2 eV from a photon energy of 3.0 eV to 3.2 eV.

In semiconductors, indirect interband transitions are characterized by a quadratic energy dependence of the optical absorption coefficient, α, near the absorption edge than is otherwise the case for direct transitions,[22] which have a square-root energy dependence. The quadratic dependence is given in eq 3

$$\alpha = B_i(h\nu - E_g)^2/h\nu \quad (3)$$

where B_i is the absorption constant for the indirect transition and E_g is the band gap. Plots of (O_2 photodesorption yield $\times$ $h\nu$)$^{1/2}$ against the excitation energy, $h\nu$, shown in Figure 7 display a linear relationship for the first four data points of each curve. This suggests that the O_2 photodesorption processes from nitrogen-implanted and from undoped TiO_2 single crystals, with intercepts at the threshold energy of 2.97 and 3.15 eV, respectively, are initiated by indirect band gap transitions in the substrate.[22,23]

IV. Discussion

Doping of polycrystalline powders and films of TiO_2 with anion impurities such as nitrogen,[10−12] sulfur,[9] and carbon[8] has been shown to be effective in lowering the threshold energy for photochemistry on the TiO_2 surface. This beneficial doping effect is explained by mixing of the N-, S-, and C-derived p states with the O 2p states leading to band gap narrowing.[8,9,11,12]

Asahi et al.[11,12] have accomplished N doping by reactive sputtering of TiO_2 film targets in N_2/Ar gas mixtures, by high-

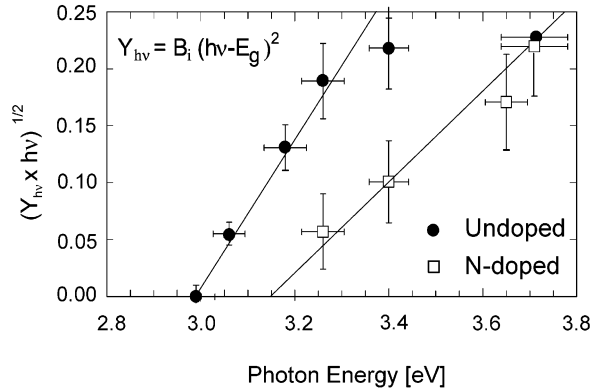

Figure 7. Plots of (O_2 photodesorption yield × $h\nu$)$^{1/2}$ vs photon energy (eV) for undoped and nitrogen-implanted TiO_2(110) crystals.

temperature treatment of TiO_2 powders in NH_3/Ar atmospheres, and by oxidative annealing of TiN powder. In all cases, a noticeable new absorption range for light at energies less than the band gap energy of 3.0 eV has been observed. The doped films were crystalline and XRD revealed the mixed structure of both rutile and anatase phases.[11] Nitrogen-doped powders produced by oxidation of polycrystalline TiN exhibited a homogeneous rutile phase.[12] The N (1s) core levels, measured with XPS, revealed three peak structures at binding energies at 402, 400, and 396 eV. Whereas the two features at higher binding energies were attributed to molecularly adsorbed nitrogen species, the nitrogen peak at 396 eV was assigned to the substitutionally bound N^- species. On the basis of a quantitative correlation between photocatalytic activity and an increase of nitrogen component related to the 396 eV peak, these authors concluded that nitrogen ions which substitute O^{2-} in the TiO_2 lattice are the photoactive dopant species. In the present study, nitrogen doping was attained by sputtering atomically clean TiO_2 single-crystal surfaces with mixtures of N_2^+ and Ar^+ ions. The SIMS profile proves that nitrogen was sucessfully implanted in the near-surface region, $0 < x < 200$ Å, and the XPS results exclusively revealed a N (1s) feature at 396.5 eV (Figure 1) due to substitutional atomic N^- species.

In general, ion bombardment of TiO_2 crystal surfaces leads to the amorphization and partial reduction of the near-surface region, because oxygen ions are preferentially sputtered due to their lower binding energy.[7] In case of exclusive sputtering with noble gas ions, a state of constant concentration for all elements (Ti, O, Ar) and all oxidation states is reached after removal of a 100 Å thick layer.[24] Subsequent annealing of the sputtered crystal to 900 K allows the epitaxial recrystallization of the amorphous and sputter-damaged area. Surface stoichiometry and structure are restored to bulklike quality due to the diffusion of interstitial Ti ions from the surface into the bulk.[25] In the present study, cross-sectional TEM images reveal a more complex state of the near-surface region. Monocrystallinity was not restored after sputtering with N_2^+ and Ar^+ ions and subsequent annealing under UHV conditions. This may be due to the presence of chemically bound atomic nitrogen, which is then involved in the recrystallization process at elevated temperature. Nitrogen incorporation into the TiO_2 lattice causes changes in the lattice parameters (i.e., strain and stress). These effects can be accommodated by the disorientation of small recrystallized grains on top and between the monocrystalline structure of the crystal bulk (Figure 4). The following estimate was done to check if nitrogen-induced stress in the TiO_2 lattice could explain the observed band gap shift: according to the literature, the pressure dependence of the band gap position for an anatase TiO_2 single crystal[26] is 10 meV/GPa and no experimental value for TiO_2 in the rutile modification was found. However, SnO_2, which has the rutile structure and is also a wide band gap oxide semiconductor, has a value of 62 meV/GPa.[27] If we assume that these two values are the lower and upper limits for the rutile phase, the required stress to produce a band gap shift of 200 meV would be 20 and 3.2 GPa, respectively. The value for compressive strength, which corresponds to the maximum compressive stress for TiO_2, is 0.245 GPa for failure.[28] This is 1 order of magnitude smaller than the calculated 3.2 GPa for SnO_2 to produce a 200 meV offset and a factor of 80 smaller if the 10 meV/GPa value for anatase is used. For this reason, we exclude strain as a possible source for the observed blueshift.

The shift of the photodesorption threshold energy by 200 meV to the blue could easily be explained by the conversion of rutile to anatase[7] by the nitrogen implantation and annealing procedure used here. In fact, it has been reported that by N^+ implantation into polycrystalline TiO_2 films, a phase transformation of crystalline rutile to anatase occurred due to the relaxation of internal strain.[29,30] In this study, XTEM images were acquired from samples of different parts of the nitrogen-implanted crystal. All of the crystalline regions that were analyzed by their Fourier transforms were determined to be rutile. Not one grain was consistent with the structure of anatase. As a consequence of these observations, the volume fraction of any anatase phase if present must be very small and therefore should not contribute to the observed change in the optical properties.

Serpone et al.[23] suggested that the observation of blueshifted thresholds, observed on small TiO_2 particles and taken as evidence for a quantum size effect, are due to direct (Franck−Condon-type) transitions in an otherwise indirect band gap semiconductor. Although such direct transitions were noted for rutile TiO_2,[31] this concept does not apply here. The action curves for undoped and nitrogen-implanted crystals display a quadratic dependence on the excitation energy, characteristic of indirect band gap transitions in both cases (Figure 7).

A well-known phenomenon associated with the optical properties of n-type semiconductors is the so-called "band-filling mechanism" (Figure 8).[32] It is based on the effect of electron concentration on the location of the Fermi level, E_f. For intrinsic or lightly doped semiconductors, such as vacuum-annealed and thermally reduced TiO_2, E_f is positioned within the band gap and the semiconductor is said to be nondegenerate. When the electron concentration in the bulk is increased, e.g., by heavy n-type doping, the semiconductor becomes degenerate and E_f lies above the bottom of the conduction band. As a consequence, some of the states within the conduction band (CB) are then filled, and electrons excited by a UV−vis photon must go into higher levels in order to enter the CB, thus leading to a blueshift in optical absorption (Figure 8). For vacuum-annealed TiO_2 crystals that are intrinsic n-type semiconductors, the local increase in partially reduced $Ti^{<4+}$ cations has a similar effect on electron concentration and, thus, on the position of E_f. Although N is considered to be a shallow p-type dopant, wide band gap semiconductors such as ZnO are difficult to p-dope using a pure nitrogen source alone. Because of ionic charge compensation, the N acceptors can easily be compensated by donor levels, which are related to additional oxygen vacancies and cations.[33] Thus, we conclude, that the implantation of N^- ions into the rutile TiO_2 lattice, substituting O^{2-} ions, also increases the local concentration of electronically reduced Ti^{3+} states due to the monovalent oxidation state of the nitrogen anion. A maximum concentration of nitrogen of about 1 atomic % corresponds to a local concentration of 10^{20}/cm^3 additional

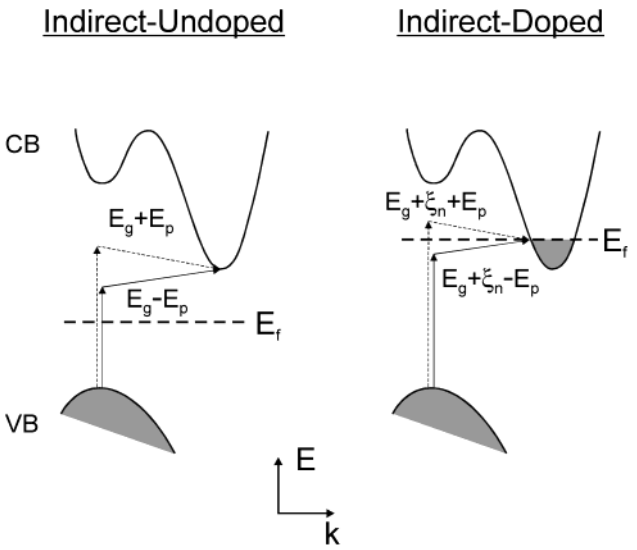

Figure 8. Schematic presentation of the effect of band filling on the photoexcitation threshold energy for a semiconductor with a band gap of E_g (adopted from ref 29). In this energy−momentum diagram for a degenerate n-type semiconductor, two phonon-assisted transitions ($E_g \pm E_p$) are shown to illustrate the usual photon absorption mechanism. If the semiconductor is heavily doped, the Fermi level, E_f, is inside the conduction band in an n-type material by a quantity ξ_n. Since the states below ξ_n are already filled, electronic transitions to states below $E_g + \xi_n$ are forbidden; hence, the absorption edge should shift to higher energies by about ξ_n.

charge carriers in the photoactive near-surface region. Alternative charge compensation based on the presence of cation vacancies is unlikely, since the sputtering process creates an overall surplus of Ti cations, which then becomes depleted through annealing via the process of bulk-assisted oxidation.[25] In conclusion, we propose that the blueshift in the action curve for O_2 photodesorption is due to a band-filling mechanism based on the increase of the n-doping level of the TiO_2 crystal by N^- incorporation.

V. Conclusions and Outlook

Reactive $N_2^+ + Ar^+$ sputtering and subsequent annealing at 900 K in UHV of a rutile TiO_2(110) single crystal leads to the implantation of atomic nitrogen within a range of 0−200 Å. The photochemical activity of nitrogen-implanted and undoped TiO_2 was investigated by means of O_2 photodesorption, and the action curve revealed, opposite to a beneficial doping effect observed on polycrystalline materials,[11,12] a blueshift compared to undoped crystals. This phenomenon is explained by the partial filling of the conduction band by electrons.

The changes in the optical properties due to the implantation of N^- into rutile single crystals may hold technological promise, since TiO_2, with its high dielectric constant, is extensively used in optical devices,[7] and tuning of its electronic properties is also important for microelectronics. The presence of a band-filling mechanism caused by N^- dopant incorporation would imply that within the modified layer the local concentration of excess electrons can also be raised by UV light. As a result, the Fermi level and thus the reduction potential of the semiconductor material becomes a function of irradiation intensity and is adjustable by the photon flux.[28,34]

Acknowledgment. This work was supported by the DoD Multidisciplinary University Research Initiative program administered by the Army Research Office under Grant DAAD-19-01-0-0619. Dr. O. Diwald gratefully acknowledges the support by the Austrian Science Fund (Project J2058). We would like to thank Mr. Tykhon Zubkov for helpful advice and direction and Dr. Alois Lugstein for fruitful discussions. Special thanks to Pittsburgh Plate Glass for use of their facilities.

References and Notes

(1) Fujishima, A.; Honda, K. *Nature* **1972**, *238*, 37.
(2) Khan, S. U. M.; Akikusa, J. *Int. J. Hydrogen Energy* **2002**, *27*, 863.
(3) O'Regan, B.; Gratzel, M. *Nature* **1991**, *353*, 737.
(4) Linsebigler, A.; Lu, G.; Yates, J. T., Jr. *Chem. Rev.* **1995**, *95*, 735.
(5) Martin, S. T.; Choi, W.; Bahnemann, D. W.; Hoffmann, M. R. *Chem. Rev.* **1995**, *95*, 69.
(6) *Photocatalysis: Fundamentals and Applications*; Serpone, N., Pilezzetti, E., Eds.; Wiley-Interscience: New York, 1989.
(7) Diebold, U. *Surf. Sci. Rep.* **2003**, *48*, 53.
(8) Khan, S. U. M.; Al-Shahry, M.; Ingler, W. B., Jr. *Science* **2002**, *297*, 2243.
(9) Umebayashi, T.; Yamaki, T.; Itoh, H.; Asai, K. *Appl. Phys. Lett.* **2002**, *81*, 454.
(10) Sato, S. *Chem. Phys. Lett.* **1986**, *123*, 126.
(11) Asahi, R.; Morikawa, T.; Ohwaki, T.; Aoki, K.; Taga, Y. *Science* **2001**, *293*, 269.
(12) Morikawa, T.; Asahi, R.; Ohwaki, T.; Aoki, K.; Taga, Y. *Jpn. J. Appl. Phys.* **2001**, *40*, L561.
(13) Linsebigler, A.; Lu, G.; Yates, J. T., Jr. *J. Phys. Chem.* **1996**, *100*, 6631.
(14) Walck, S. D.; McCaffrey, J. P. *Mater. Res. Soc. Symp. Proc.* **1997**, *480*, 149.
(15) Prior work done by sputtering with nitrogen alone showed that nitrogen was incorporated, but after postannealing, significant nitrogen loss was observed. Using a heavier ion in conjunction with nitrogen allows for a more persistent implantation of the dopant through utilization of the so-called "knock on effect".
(16) Saha, N. C.; Tompkins, H. G. *J. Appl. Phys.* **1992**, *72*, 3072.
(17) The effects seen in the first 50 Å are representative for the pre-equilibrium region of the sputtering process and are ascribed to SIMS-specific phenomena arising from primary ion mixing and the chemical enhancement of the secondary ion yield. See: Wilson, R.; Stevie, F.; Magee, C. In *Secondary Ion Mass Spectrometry*; Wiley and Sons: 1989; and Williams, P. In *Secondary Ion Mass Spectrometry SIMS*; Wiley and Sons: 1998; Vol. XI, pp 3−10.
(18) T. Roch, Institute for Solid State Electronics, Technical University of Vienna, private communication.
(19) Pan, J. M.; Maschhoff, B. L.; Diebold, U.; Madey, T. E. *J. Vac. Sci. Technol., A* **1992**, *10*, 2470.
(20) Diebold, U.; Lehman, J.; Mahmound, T.; Kuhn, M.; Leonardelli, G.; Hebenstreit, W.; Schmid, M.; Varga, P. *Surf. Sci.* **1998**, *411*, 137.
(21) Henderson, M. A.; Epling, W. S.; Perkins, C. L.; Peden, C. H. F.; Diebold, U. *J. Phys. Chem. B* **1999**, *103*, 5328.
(22) Mooser, E.; Pearson, W. B. In *Progress in Semiconductors*; Gibson, A. F., Ed.; John Wiley & Sons: New York, 1960; Vol 5, p 53.
(23) Serpone, N.; Lawless, D.; Khairutdinov, R. *J. Phys. Chem.* **1995**, *99*, 16646 and references therein.
(24) Wolff, M.; Schultze, J. W. *Surf. Interface Anal.* **1988**, *12*, 93.
(25) Henderson, M. A. *Surf. Sci.* **1999**, *419*, 174.
(26) Ohta, S.; Sekiya, T.; Kurita, S. *Phys. Status Solidi B* **2001**, *223*, 265.
(27) Schweitzer, C.; Reimann, K.; Steube, M. *Solid State Commun.* **1999**, *110*, 697.
(28) Samsonov, G. V. *The Oxide handbook*; IFI/Plenum: New York, 1973.
(29) Fukushima, K.; Yamada, I. *Jpn. J. Appl. Phys.* **1996**, *35*, 5790.
(30) Fukushima, K.; Yamada, I. *Nucl. Instrum. Methods Phys. Res., Sect. B* **1996**, *112*, 116.
(31) Ghosh, A. K.; Wakim, F. G.; Adiss, P. R. *Phys. Rev.* **1969**, *30*, 433.
(32) Pankove, J. I. *Optical processes in semiconductors*; Dover Publications: New York, 1975; p 39.
(33) Lee, E.-C.; Kim, Y.-S.; Jin, Y.-G.; Chang, K. J. *Phys. Rev. B* **2001**, *64*, 085120.
(34) Liu, C.-Y.; Bard, A. J. *J. Phys. Chem.* **1989**, *93*, 3232.